Energy Storage and Saving 3 (2024) 87–95

Contents lists available at ScienceDirect

Energy Storage and Saving

journal homepage: www.keaipublishing.com/en/journals/energy-storage-and-saving/

Energy, exergy, and economic analysis of compression-absorption cascade refrigeration cycle using different working fluids

Yuhan Du, Chenhan Chi, Xiaopo Wang *

Key Laboratory of Thermo-Fluid Science and Engineering, Ministry of Education, Xi'an Jiaotong University, Xi'an, 710049, China

ARTICLE INFO

Keywords:
Compression-absorption cascade refrigeration cycle
Working fluids
Economic analysis
Multi-objective optimization

ABSTRACT

Compression-absorption cascade refrigeration cycle (CACRC) combined with vapor-compression refrigeration and absorption refrigeration cycle attracts great interest due to the less electricity consumption and utilization waste heat. In this work, the performance of the CACRC system was investigated using 16 refrigerants in the vapor compression section and H_2O-LiBr in the absorption refrigeration section. Energy, exergy and economic analysis of the CACRC system were carried out and the results were compared. Results show that RE170/H_2O-LiBr presents the better coefficient of performance and exergy efficiency amongst all the studied fluids. In addition, the economic optimization, multi-objective optimization, and thermodynamic optimization of the CACRC system based on the RE170/H_2O-LiBr working fluid were also carried out.

1. Introduction

The vapor-compression refrigeration (VCR) and absorption refrigeration cycle (ARC) are two typical cooling ways. Generally speaking, the VCR has higher performance and can achieve a low refrigerating temperature. However, the VCR consumes a large quantity of electrical energy. Meanwhile, ARC can be driven by waste heat source, and the electricity consumed is very low. Hence, for the purpose of complementary advantage, the compression-absorption cascade refrigeration cycle (CACRC) combined with VCR and ARC was proposed [1], it attracts more and more interest because of the good potential applications, such as food industry or district cooling [2,3].

In the last few years, the investigations on the performance of the CACRC system have been reported by many researchers [4,5]. The existing studies can generally be divided into two categories. One is focusing on the different configurations of the system. The conventional CACRC system is a combination of an ideal VCR and a single stage ARC through a cascade heat exchanger. Subsequently, several advanced CACRC configurations with improved ARC cycle (e.g. double stage, triple stage) and VCR cycle (e.g. ejector-based VCR, adding throttle) was proposed and analyzed [6–8]. Except for the system modification, the evaluation of different working fluids used in VCR and ARC sections is also essential for the CACRC system.

The working pairs of NH_3-H_2O and H_2O-LiBr were widely used in the ARC cycle. For NH_3-H_2O pair, the rectifier should be used and this can increase the complexity of the cycle [9]. Seyfouri and Ameri [10] reported that the CACRC system using NH_3-H_2O pair requires higher pump power because of higher generator temperature and higher pressure. Moreover, Cimsit and Ozturk [2] compared the performance of CACRC system using H_2O-LiBr and NH_3-H_2O in the absorption section, respectively. Results show that the thermal energy consumption of the system with H_2O-LiBr pair decreases by 35% and COP increases by 33% compared to NH_3-H_2O at the same cooling capacity. In this regard, H_2O-LiBr is a good choice for the absorption section of CACRC system.

In case of the vapor compression section in the CACRC system (H_2O-LiBr in the ARC), Cimsit et al. [11] compared the energy and exergy efficiency of four refrigerants (R717, R744, R410A and R134a) and R717/H_2O-LiBr shows the best performance. Colorado and Velazquez [12] simulated CACRC system which added an internal heat exchanger in the VCR section and compared the performance of R717, R134a and R744. The results indicate that R134a/H_2O-LiBr has the highest COP. Salhi et al. [13] conducted thermodynamic and thermo-economic analysis of a geothermal-assisted CACRC system operated with R1234yf, R1234ze(E) and R1233zd(E) in the vapor compression section. They found that the system using R1234yf/H_2O-LiBr gets the better performance. Turgut and Turgut [14] compared the performance of CACRC system using R1234yf, R134a, R717 and R290. It was found that R717/H_2O-LiBr has the lowest total annual cost while R290/H_2O-LiBr can obtain the maximum second law efficiency.

Although the investigations on the performance of the CACRC system using different refrigerants have been reported; however, some of the

* Corresponding author.
E-mail address: wangxp@xjtu.edu.cn (X. Wang).

https://doi.org/10.1016/j.enss.2024.02.003
Received 15 December 2023; Received in revised form 20 February 2024; Accepted 20 February 2024
Available online 21 February 2024

Nomenclature

A	Heat transfer area (m^2)
a^c	Capital recovery factor
C_{CO2}	Unit damage cost of CO_2 emission ($\$\cdot kg^{-1}$)
C_{ele}	Unit cost of electrical exergy ($\$\cdot(kW\cdot h)^{-1}$)
C_{env}	Penalty or social cost of CO_2 emission ($\$\cdot(kW\cdot h)^{-1}$)
C_f	Unit cost of fuel exergy ($\$\cdot(kW\cdot h)^{-1}$)
C_p	Specific heat ($kJ\cdot(kg\cdot K)^{-1}$)
C_T	Total annual product cost ($k\$\cdot year^{-1}$)
COP	Coefficient of performance
Dev	Relative deviation
e	Specific exergy ($kJ\cdot kg^{-1}$)
$\dot{E}$	Exergy flow rate (kW)
$\dot{E}_{dest}$	Exergy destruction (kW)
h	Specific enthalpy ($kJ\cdot kg^{-1}$)
i	Annual interest rate
$\dot{m}$	Mass flow rate ($kg\cdot s^{-1}$)
N	System life time (year)
P	Pressure (kPa)
$\dot{Q}$	Heat transfer rate (kW)
R	Universal gas constant ($J\cdot(mol\cdot K)^{-1}$)
s	Specific entropy ($kJ\cdot(kg\cdot K)^{-1}$)
T	Temperature (K)
t_{op}	Hours of operation per year (h)
U	Overall heat transfer coefficient ($kW\cdot(m^2\cdot K)^{-1}$)
$\dot{W}$	Power (kW)
X	LiBr mass concentration
y_i	Mole fraction of LiBr
Z	Investment cost ($)
ΔT	Temperature difference (K)

Greek symbols

η	Efficiency
ε	Effectiveness of solution heat exchanger
Φ	Maintenance factor
λ	Emission conversion factor of electricity ($\$\cdot(kW\cdot h)^{-1}$)

Subscripts

0	Environmental condition
1,2…22	State points
ARC	Absorption refrigeration cycles
b	Normal boiling point
c	Critical condition
ch	Chemical exergy
e	Electrical efficiency
exg	Exergy efficiency
is	Isentropic efficiency
k	kth component of system
ph	Physical exergy
pre	Present model
ref	Reference model
VCRC	Vapor compression refrigeration cycles

Superscripts

C	Cold side
H	Hot side

Abbreviation

ABS	Absorber
CACRC	Compression-absorption cascade refrigeration cycles
CHE	Cascade heat exchanger
COM	Compressor
CON	Condenser
EVA	Evaporator
EXV	Expansion valve
GEN	Generator
LMTD	Logarithmic mean temperature difference
NSGA-II	Non-dominated Sorting Genetic Algorithms-II
SHE	Solution heat exchanger

studied refrigerants (e.g., R134a and R410a) in the VCR section of the CACRC system have higher global warming potential (GWP) value. In addition, there is no systematical comparison of the whole potential refrigerants that used in the CACRC system until now. In this work, the performance of the traditional CACRC system was further compared considering 16 refrigerants (especially for low GWP refrigerants) used in the VCR section, and H_2O-LiBr working pair was used in the ARC section. The effects of the key operating parameters including generator temperature, evaporator temperature, cascade temperature difference and solution heat exchanger effectiveness on the system performance were analyzed. In addition, the results of three optimization scenarios (the single-objective thermodynamic optimization, the single-objective economic optimization, and the multi-objective optimization) achieved by non-dominated sorting genetic algorithms-II (NSGA-II) were analyzed for the CACRC system.

2. CACRC system and mathematic model

The schematic diagram of the traditional CACRC system is illustrated in Fig. 1. The main components include generator (GEN), condenser (CON), absorber (ABS), solution heat exchanger (SHE), cascade heat exchanger (CHE), evaporator (EVA), compressor (COM), pump, and three expansion valves (EXV).

In the absorption refrigeration section, weak solution (point 10) is separated as superheated water vapor (point 14) and strong solution (point 11) in the generator. Then water vapor is condensed to the saturated liquid state in the condenser. After throttled in the expansion valve 1, the two-phase stream (point 6) gains heat from the cascade heat exchanger and becomes saturated vapor state (point 7). The vapor is then absorbed into the strong solution in the absorber. The weak solution (point 8) is pumped into solution heat exchanger to recover the heat from the strong solution before entering the generator. After the heat is released in the solution heat exchanger, the strong solution (point 12) passes through the expansion valve 3 and flows toward the absorber. In the vapor compression section, saturated refrigerant vapor (point 1) is compressed in the compressor and cooled to saturated liquid state (point 3) in the cascade heat exchanger. Finally, it is throttled across the expansion valve 2 and absorbs heat from chilled air to produce cold energy for user.

For the analysis of CACRC system, several assumptions are taken into consideration in this work:

(1) Each control volume is at steady state condition.
(2) The refrigerant at points 1, 3, 5 and 7 is saturated. Both the strong solution (point 11) and weak solution (point 8) leaving the generator and absorber are saturated.
(3) The heat transfer between CACRC system and environment is ignored. The pressure drop in the pipelines and heat exchangers as well as the power consumption of the solution pump are neglected.
(4) All expansion valves are isenthalpic.

Based on the above assumptions, the mass and energy balance are applied for each component in CACRC system. The common equations

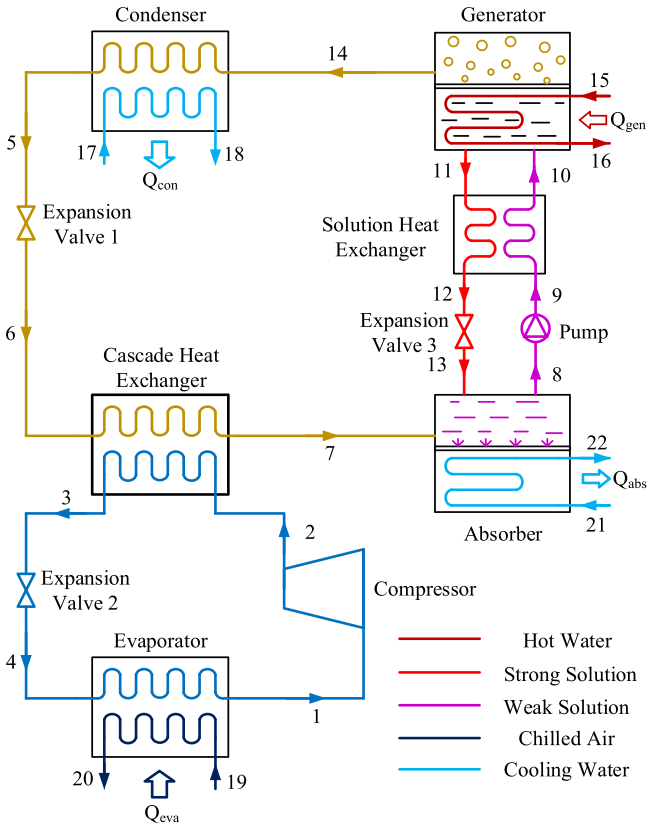

Fig. 1. Schematic diagram of the CACRC system.

are expressed as [15]:

$$\text{Mass balance}: \sum \dot{m} = 0 \tag{1}$$

$$\text{Energy balance}: \sum \dot{Q} + \sum \dot{W} = \sum \dot{m}_{\text{out}} h_{\text{out}} - \sum \dot{m}_{\text{in}} h_{\text{in}} \tag{2}$$

For the solution heat exchanger in the absorption refrigeration section, the effectiveness ε is an important parameter, it is defined as the ratio of actual heat transfer to the maximum possible heat transfer [16]:

$$\varepsilon = \frac{h_{11} - h_{12}}{h_{11} - h_{12^*}} \tag{3}$$

where h_{12^*} represents the enthalpy of strong solution at the exit of the solution heat exchanger when it is cooled to the temperature of point 9.

The heat input from the hot water in the generator is expressed as:

$$\dot{Q}_{\text{GEN}} = \dot{m}_{11} \cdot h_{11} + \dot{m}_{14} \cdot h_{14} - \dot{m}_{10} \cdot h_{10} \tag{4}$$

The heating capacity of the condenser, absorber and cascade heat exchanger are given by:

$$\dot{Q}_{\text{CON}} = \dot{m}_5 \cdot (h_{14} - h_5) \tag{5}$$

$$\dot{Q}_{\text{ABS}} = \dot{m}_7 \cdot h_7 + \dot{m}_{13} \cdot h_{13} - \dot{m}_8 \cdot h_8 \tag{6}$$

$$\dot{Q}_{\text{CHE}} = \dot{m}_6 \cdot (h_7 - h_6) = \dot{m}_2 \cdot (h_2 - h_3) \tag{7}$$

The refrigeration output in the evaporator is described as:

$$\dot{Q}_{\text{EVA}} = \dot{m}_1 \cdot (h_1 - h_4) \tag{8}$$

The isentropic efficiency and power consumption for the compressor are:

$$\eta_{\text{is,COM}} = \frac{h_{2s} - h_1}{h_2 - h_1} \tag{9}$$

$$\dot{W}_{\text{COM}} = \dot{m}_1 \cdot (h_2 - h_1) / \eta_{\text{e,COM}} \tag{10}$$

where $\eta_{\text{e,COM}}$ represents electrical efficiency of the compressor and is taken as 0.90 [2].

The coefficient of performance of the absorption section:

$$\text{COP}_{\text{ARC}} = \dot{Q}_{\text{CHE}} / \dot{Q}_{\text{GEN}} \tag{11}$$

The coefficient of performance of the compression section:

$$\text{COP}_{\text{VCR}} = \dot{Q}_{\text{EVA}} / \dot{W}_{\text{COM}} \tag{12}$$

The overall coefficient of performance of the CACRC system:

$$\text{COP}_{\text{CACRC}} = \dot{Q}_{\text{EVA}} / (\dot{Q}_{\text{GEN}} + \dot{W}_{\text{COM}}) \tag{13}$$

The exergy balance equation is established and the expression is:

$$\dot{E}_{\text{dest}} = \sum_{\text{in}} \dot{m}e - \sum_{\text{out}} \dot{m}e - \sum \dot{Q}\left(1 - \frac{T_0}{T}\right) + \sum \dot{W} \tag{14}$$

When calculating exergy value of stable flowing LiBr solution in a component, kinetic and potential components of exergy are ignored, only physical exergy and chemical exergy are considered, and the expression is:

$$e = e_{\text{ph}} + e_{\text{ch}} \tag{15}$$

Physical exergy is calculated based on:

$$e_{\text{ph}} = (h - h_0) - T_0(s - s_0) \tag{16}$$

where h_0 and s_0 are specific enthalpy which refers to the steady flow under environmental temperature and pressure conditions.

Chemical exergy is calculated as [2,13]:

$$e_{\text{ch}} = RT_0 \ln y_i \tag{17}$$

where R is universal gas constant, y_i is mole fraction.

The exergy efficiency of the CACRC system is expressed as:

$$\eta_{\text{exg}} = \frac{\dot{Q}_{\text{EVA}} \left| 1 - \left(\frac{2T_0}{T_{19} + T_{20}} \right) \right|}{\dot{Q}_{\text{GEN}} \left[1 - \left(\frac{2T_0}{T_{15} + T_{16}} \right) \right] + \dot{W}_{\text{COM}}} \tag{18}$$

The detailed energy and exergy balance equations for each component are given in Supplementary material. The properties of water and the studied refrigerants are obtained from REFPROP 10.0 [17], and the enthalpy and entropy of LiBr solution are calculated using the formulas proposed by Patek and Klomfar [18].

In order to evaluate the quality of the system, the economic performance was analyzed in this work. The economic analysis considers the operational cost, including the cost of fuel input to the generator and the cost of electricity consumed by compressor, the investment and maintenance cost and penalty or social cost of CO_2 emission. The total annual product cost is given by Jain et al. [19]:

$$C_{\text{T}} = t_{\text{op}} \left(C_{\text{f}} \dot{Q}_{\text{GEN}} + C_{\text{ele}} \dot{W}_{\text{COM}} \right) + a^c \phi \sum_{\text{k} \in \text{EQS}} Z_{\text{k}} + C_{\text{env}} \tag{19}$$

$\forall$ k $\in$ EQS $\cap$ {GEN, CON, ABS, CHE, SHE, EVA, COM} where the unit cost of fuel exergy (C_{f}) and electrical exergy (C_{ele}) are supposed to be 0.03785 \$·(kW·h)$^{-1}$ [19,20] and 0.075 \$·(kW·h)$^{-1}$ [21], respectively. In addition, the system operates (t_{op}) 5,000 h annually [19,20]. The maintenance factor (Φ) is assumed to be 1.06 [22]. Furthermore, the capital recovery factor (a^c) is considered as follows:

$$a^c = \frac{i(1+i)^N}{(1+i)^N - 1} \tag{20}$$

where annual interest rate (i) and life time (N) are assumed to be 0.15 and 10 years [19], respectively.

Table 1
Comparison of the present model with the reference for CACRC system.

Parameters	R134a/H_2O-LiBr			R717/H_2O-LiBr			R410a/H_2O-LiBr		
	Ref.	This work	Dev (%)	Ref.	This work	Dev (%)	Ref.	This work	Dev (%)
$\dot{Q}_{GEN}$ (kW)	76.45	76.87	0.546	76.45	76.74	0.382	76.76	77.20	0.571
$\dot{Q}_{CHE}$ (kW)	57.41	57.55	0.247	57.3	57.46	0.276	57.72	57.80	0.138
$\dot{Q}_{ABS}$ (kW)	72.76	73.21	0.616	72.76	73.09	0.452	73.06	73.52	0.634
$\dot{Q}_{CON}$ (kW)	61.06	61.21	0.248	61.06	61.11	0.084	61.31	61.48	0.269
$\dot{W}_{COM}$ (kW)	8.25	8.39	1.706	8.08	8.29	2.556	8.58	8.67	1.003
COP_{ARC}	0.750	0.749	0.172	0.75	0.749	0.172	0.750	0.749	0.172
COP_{VCR}	6.061	5.959	1.684	6.188	6.034	2.490	5.827	5.770	0.984
COP_{CACRC}	0.59	0.586	0.601	0.592	0.588	0.669	0.586	0.582	0.629

In this work, the investment costs of all the heat exchangers and compressor are considered, and the costs of pump, expansion valves and connecting pipes are ignored [23]. The cost of heat exchanger mainly depends on its heat transfer area (A_k), which can be calculated from the following expression:

$$\dot{Q}_k = U_k \cdot A_k \cdot LMTD_k \tag{21}$$

$\forall$ k $\in$ EQS $\cap$ {GEN, CON, ABS, CHE, SHE, EVA} where $LMTD_k$ is the logarithmic mean temperature difference, and the expression is:

$$LMTD_k = \frac{\Delta T_k^H - \Delta T_k^C}{\ln \frac{\Delta T_k^H}{\Delta T_k^C}} \tag{22}$$

where ΔT_k^H and ΔT_k^C are the temperature differences on both hot and cold sides, respectively [24,25]. The detailed *LMTD* and overall heat transfer coefficient (U_k) for each heat exchanger in CACRC system are listed in Supplementary material.

The investment cost of heat exchanger is:

$$Z_k = 516.621 A_k + 268.45 \tag{23}$$

The capital cost of compressor can be expressed as:

$$Z_{COM} = \left(\frac{573 m_1}{0.8996 - \eta_{is,COM}}\right)\left(\frac{P_2}{P_1}\right)\ln\left(\frac{P_2}{P_1}\right) \tag{24}$$

The penalty or social cost of the CO_2 emission is considered as important environmental criteria in this work, which is estimated based on the following equation [26]:

$$C_{env} = \lambda \dot{W}_{COM} t_{op} C_{CO_2} \tag{25}$$

wherein, the emission conversion factor of electricity from grid (λ) and the unit damage cost of CO_2 emission (C_{CO_2}) are taken as 0.968 \$·(kW·h)$^{-1}$ [22,27] and 90,000 \$·kg^{-1} [19], respectively.

In order to validate the correctness of the model, the calculated results from the model were compared with the work of Cimsit and Ozturk [2]. The input parameters are Q_{EVA}=50 kW, T_{GEN}=363 K, T_{CON}=T_{ABS}=313 K, T_{EVA}=263 K, T_7=283 K, ΔT_{CHE}=8 K, ε_{SHE}=0.6, $\eta_{is,COM}$=0.8 and $\eta_{e,COM}$=0.9. The relative deviation was calculated from:

$$Dev = 100\frac{|R_{ref} - R_{pre}|}{R_{ref}} \tag{26}$$

Table 1 shows the comparison results of the present model with the work of Cimsit and Ozturk [2] for CACRC system. H_2O-LiBr is chosen for the absorption refrigeration section, and R134a, R717 and R410a are selected for the vapor compression section. It is obvious that the calculated results of the present model are quite close to the literature.

3. Results and discussion

3.1. Calculated results from 16 refrigerants

Considering the restriction of the environmental characteristics, the low GWP refrigerants were chosen in this work. In addition, for comparison purpose, R134a, R245fa and R124 with high GWP were also included. The fundamental properties of the 16 refrigerants are given in Table 2. The studied refrigerants can be classified into three groups according to the slope of saturated vapor curve in the *T-s* diagram: dry fluids (positive-slope, including R600a, R600 and R245fa), isotropic fluids (nearly infinite-slope, including R1234yf, R1243zf, R1234ze(E) and R124) and wet fluids (negative-slope, including R744, R170, R32, R1270, R290, R134a, R152a, RE170 and R717).

Table 2
Properties of the studied refrigerants [17,28,29].

Substance		T_b (K)	T_c (K)	P_c (MPa)	ODP	GWP	Safety group
1	R744	194.69	304.15	7.38	0	1	A1
2	R170	184.57	305.35	4.87	0	~20	A3
3	R32	221.55	351.25	5.78	0	675	A2L
4	R1270	225.46	365.57	4.665	0	~20	A3
5	R1234yf	243.7	367.85	3.382	0	4	A2L
6	R290	231.06	369.83	4.247	0	~20	A3
7	R134a	247.08	374.21	4.059	0	1430	A1
8	R1243zf	247.95	378.65	3.74	0	<150	-
9	R1234ze (E)	254.18	382.55	3.64	0	6	-
10	R152a	249.13	386.41	4.517	0	124	A2
11	R124	261.19	395.43	3.624	0.02	609	A1
12	RE170	248.37	400.35	5.34	0	0.1	A3
13	R717	239.82	405.4	11.333	0	<1	B2L
14	R600a	261.4	407.85	3.63	0	~20	A3
15	R600	272.6	425.13	3.796	0	~20	A3
16	R245fa	288.05	427.2	3.64	0	1030	B1

Table 3
Input parameters under the design condition.

Items	Units	Values	Items	Units	Values
P_0	kPa	101.325	ΔT_{CON}	K	8
T_0	K	298.15	ΔT_{ABS}	K	8
$\dot{Q}_{EVA}$	kW	250	ΔT_{EVA}	K	8
T_{GEN}	K	363.15	ΔT_{CHE}	K	8
T_7	K	283.15	ε_{SHE}	-	0.7
T_{EVA}	K	263.15	$\eta_{is,COM}$	-	0.8
ΔT_{GEN}	K	8	$\eta_{e,COM}$	-	0.9

The input parameters for the CACRC system and calculated results using the 16 refrigerants are listed in Tables 3 and 4, respectively.

Fig. 2 shows COP and exergy efficiency of the CACRC system sorted by critical temperature of the refrigerants. As presented in Fig. 2(a), for dry fluids, COP and exergy efficiency are increasing with critical temperature, and R245fa shows the highest. It is observed from Fig. 2(b) that COP and exergy efficiency are increasing with critical temperature except R1234ze(E) for isotropic fluids. Although the critical temperature of R1234ze(E) is slightly higher than R1243zf, its latent heat of vaporization is much lower than R1243zf, resulting lower COP and exergy efficiency. As shown in Fig. 2(c), with critical temperature increasing,

Table 4
Calculated results of the compression-absorption cascade refrigeration cycle (CACRC) system using 16 working fluids (sorted by critical temperature).

	R744	R170	R32	R1270	R1234yf	R290	R134a	R1243zf
$\dot{Q}_{GEN}$ (kW)	376.77	376.81	363.62	363.21	363.93	363.09	362.65	362.78
$\dot{Q}_{CHE}$ (kW)	298.95	298.98	288.52	288.19	288.76	288.10	287.74	287.85
$\dot{Q}_{ABS}$ (kW)	357.89	357.93	345.40	345.01	345.69	344.90	344.48	344.61
$\dot{Q}_{CON}$ (kW)	317.83	317.86	306.73	306.39	306.99	306.29	305.91	306.03
$\dot{W}_{COM}$ (kW)	54.39	54.43	42.80	42.44	43.07	42.33	41.94	42.06
COP_{ARC}	0.794	0.794	0.794	0.794	0.794	0.794	0.794	0.794
COP_{VCRC}	4.597	4.593	5.842	5.891	5.805	5.906	5.961	5.944
COP_{CACRC}	0.580	0.580	0.615	0.616	0.614	0.617	0.618	0.618
η_{exg}	0.207	0.207	0.232	0.233	0.232	0.233	0.234	0.234
-	R1234ze(E)	R152a	R124	RE170	R717	R600a	R600	R245fa
$\dot{Q}_{GEN}$ (kW)	362.86	361.73	362.38	361.47	362.05	362.14	361.60	361.58
$\dot{Q}_{CHE}$ (kW)	287.91	287.02	287.53	286.81	287.27	287.35	286.91	286.90
$\dot{Q}_{ABS}$ (kW)	344.68	343.61	344.22	343.36	343.91	344.00	343.48	343.46
$\dot{Q}_{CON}$ (kW)	306.09	305.14	305.69	304.92	305.41	305.49	305.03	305.01
$\dot{W}_{COM}$ (kW)	42.12	41.13	41.70	40.91	41.41	41.50	41.01	41.00
COP_{ARC}	0.794	0.794	0.794	0.794	0.794	0.794	0.794	0.794
COP_{VCRC}	5.935	6.078	5.995	6.112	6.037	6.025	6.096	6.098
COP_{CACRC}	0.617	0.621	0.619	0.621	0.620	0.619	0.621	0.621
η_{exg}	0.234	0.236	0.235	0.237	0.236	0.236	0.237	0.237

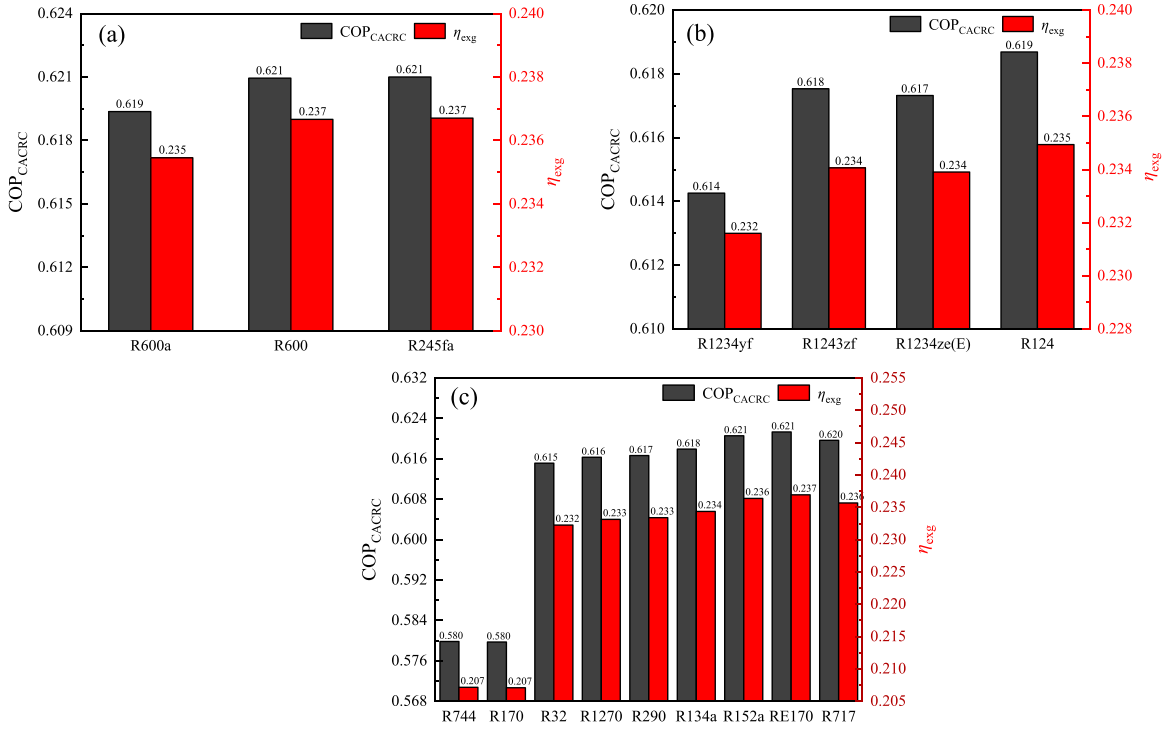

Fig. 2. COP_{CACRC} and exergy efficiency for 16 refrigerants (every group is sorted by critical temperature); (a) Dry fluids; (b) isotropic fluids; (c) wet fluids.

COP and exergy efficiency also show upward tendency except R170 and R717 for wet fluids. R744 has lower specific heat capacity than R170, resulting in higher COP and exergy efficiency of R744. Because specific heat capacity of R717 is much higher than other wet fluids, it may present different characteristics with other wet fluids [30].

Overall, the larger exergy efficiency of the system for the studied substances is RE170/H_2O-LiBr and R245fa/H_2O-LiBr. Due to the high GWP value of R245fa, RE170 (dimethyl ether, C_2H_6O) can be considered as a potential fluid. Hence, the analysis of the CACRC system using RE170/H_2O-LiBr pair was further carried out in this work. Table 5 lists the calculated results of each state point under the design condition using RE170.

3.2. Analysis of the CACRC system using RE170/H_2O-LiBr pair

3.2.1. Effect of generator temperature on the performance of the system

Fig. 3 shows the effect of generator temperature on the performance of the system at the following conditions: T_{CON}=T_{ABS}=308.15 K, T_{EVA}=263.15 K, T_7=283.15 K, ΔT_{CHE}=8 K and ε_{SHE}=0.7.

As presented in Fig. 3(a), with the increasing of T_{GEN}, the heat input of generator decreases rapidly to minimum and then increases very slightly. The concentration difference between the strong solution and weak solution increases with the increasing of generator temperature, hence, a smaller strong solution mass flow rate is required to produce the same mass of water vapor. This is the reason that the heat input of generator decreases firstly. However, the mass flow rate of the strong solution tends to a stable value at higher generator temperature. It is also

Table 5
The calculated results for each state point under the design condition using RE170.

State	T (K)	p (kPa)	X_{LiBr}	m (kg·s^{-1})	h (kJ·kg^{-1})	s (kJ·(kg·K)$^{-1}$)
1	263.15	185.031	-	0.6545	481.07	1.8314
2	307.938	479.735	-	0.6545	537.32	1.8683
3	291.15	479.735	-	0.6545	99.09	0.3658
4	263.15	185.031	-	0.6545	99.09	0.3798
5	308.15	5.629	-	0.1209	146.63	0.5051
6	283.15	1.228	-	0.1209	146.63	0.5205
7	283.15	1.228	-	0.1209	2519.21	8.8998
8	308.15	1.228	0.5219	0.6224	76.12	0.2313
9	308.15	5.629	0.5219	0.6224	76.12	0.2313
10	333.812	5.629	0.5219	0.6224	130.73	0.4014
11	363.15	5.629	0.6477	0.5015	239.65	0.4753
12	325.095	5.629	0.6477	0.5015	171.88	0.2776
13	325.095	1.228	0.6477	0.5015	171.88	0.2776
14	363.15	5.629	-	0.1209	2669.02	8.6637
15	381.15	101.325	-	0.1584	2692.09	7.3983
16	371.15	101.325	-	0.1584	410.74	1.2846
17	300.15	101.325	-	14.5898	113.28	0.3952
18	305.15	101.325	-	14.5898	134.18	0.4642
19	271.15	101.325	-	49.7206	397.27	3.7850
20	266.15	101.325	-	49.7206	392.25	3.7663
21	300.15	101.325	-	16.4290	113.28	0.3952
22	305.15	101.325	-	16.4290	134.18	0.4642

observed that there is little change in the power consumption of compressor. This is because that the mass flow rate and pressure ratio of the compressor do not change. Based on above reasons, COP of the CACRC system shows a trend of increase and then decrease slowly.

Fig. 3(b) displays the effect of T_{GEN} on exergy efficiency and total annual product cost of the system. Since the power consumption of compressor remains stable, the variation trend of exergy efficiency is contrary to that of the heat input of generator. Increasing T_{GEN} can cause the investment cost reduction of generator, absorber, and solution heat exchanger. In addition, the temperature of water vapor (point 14) raises with the increasing of T_{GEN}, leading to the investment cost growth of condenser. This can be explained that total annual product cost of the system decreases rapidly to minimum and then remains constant.

3.2.2. *Effect of evaporator temperature on the performance of the system*

The effect of evaporator temperature on the performance of the system is indicated in Fig. 4 at the following conditions: T_{GEN}=363.15 K, T_{CON}=T_{ABS}=308.15 K, T_7=283.15 K, ΔT_{CHE}=8 K and ε_{SHE}=0.7.

As can be seen in Fig. 4(a), the power consumption of compressor decreases with the increasing of T_{EVA}. The reason is that the mass flow rate of the refrigerants in the compression section decreases and the inlet pressure of compressor increases with T_{EVA} when the cooling capacity remains unchanged. Since the mass flow of water vapor required for the absorption section is reduced, the heat input of generator decreases with T_{EVA}. The heat input of generator and the power consumption of compressor are reduced simultaneously, COP of the CACRC system shows an increasing trend.

Fig. 4(b) shows the effect of T_{EVA} on exergy efficiency and total annual product cost of the system. Although the heat input of generator and the power consumption of compressor decrease with T_{EVA}, the cooling capacity of the compression section is larger than them. Therefore, the numerator of Eq. (18) plays a major role in the process of calculating exergy efficiency. Under the premise that ΔT_{EVA} is constant,

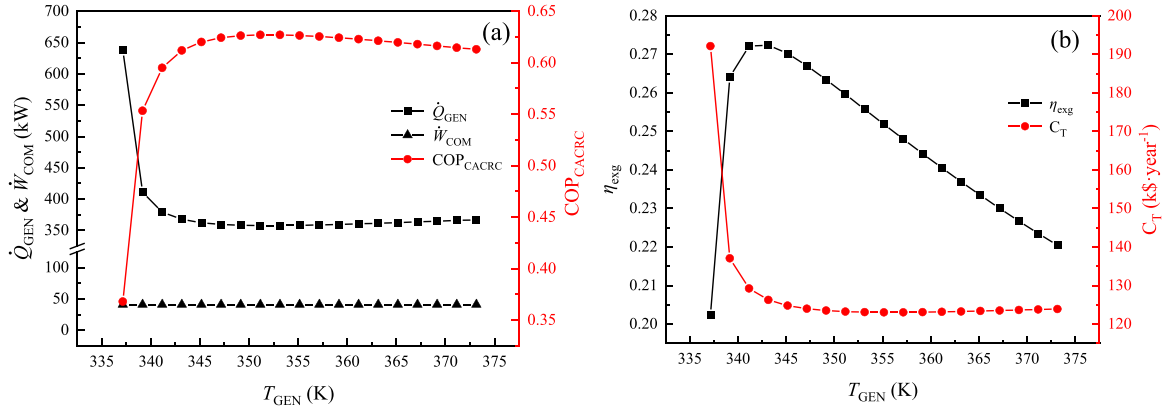

Fig. 3. The effect of generation temperature on (a) the heat input of generator, the power consumption of compressor and coefficient of performance (b) exergy efficiency and total annual product cost of the system.

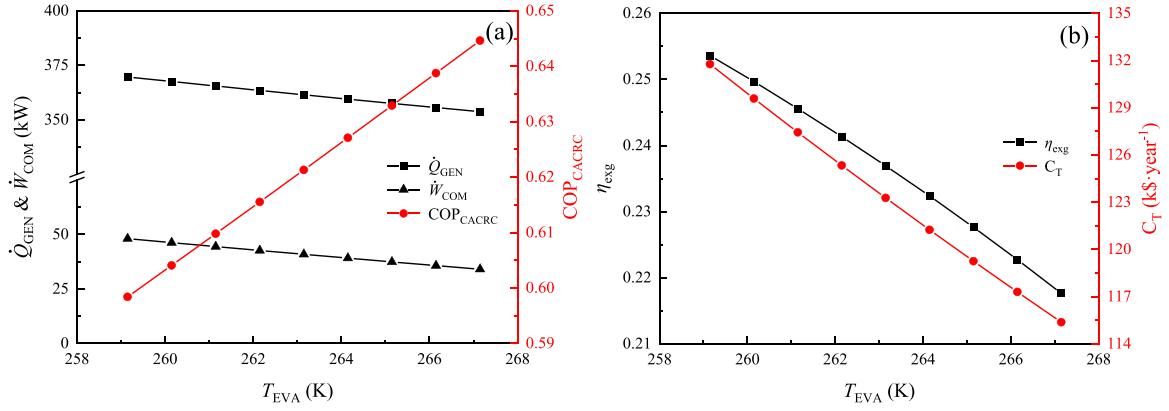

Fig. 4. Effect of evaporator temperature on (a) the heat input of generator, the power consumption of compressor and coefficient of performance, (b) exergy efficiency and total annual product cost of the system.

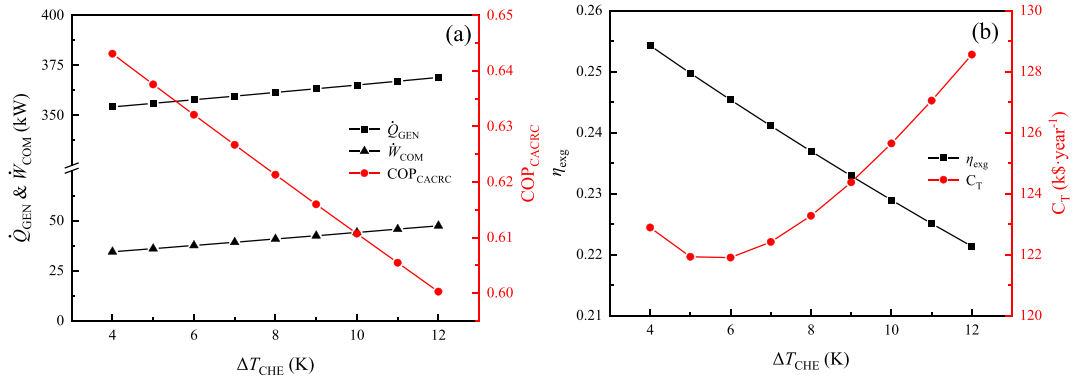

Fig. 5. Effects of cascade temperature difference on (a) the heat input of generator, the power consumption of compressor and coefficient of performance, (b) exergy efficiency and total annual product cost of the system.

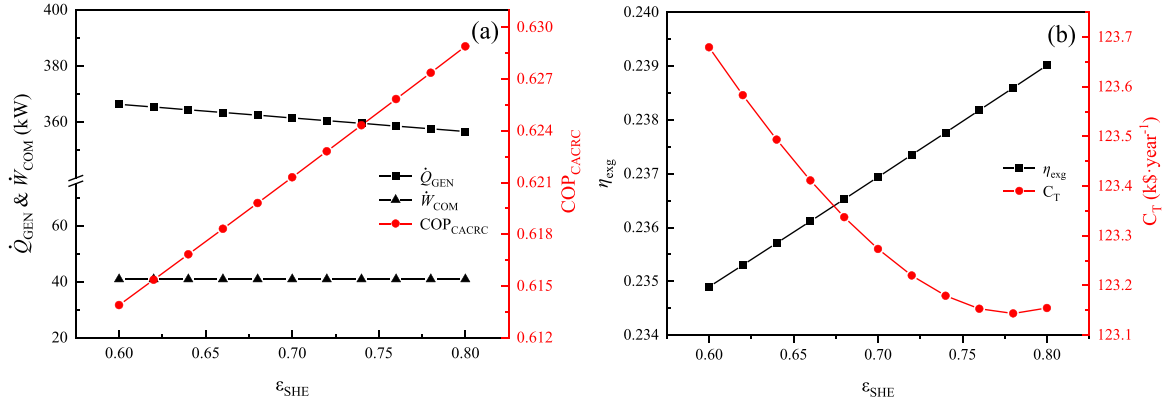

Fig. 6. Effect of solution heat exchanger effectiveness on (a) heat input of generator, the power consumption of compressor and coefficient of performance, (b) exergy efficiency and total annual product cost of the system.

the temperature of chilled air in and out evaporator increases with T_{EVA}, resulting in exergy efficiency decreasing. In addition, total annual product cost of the system decreases with the increment of T_{EVA}. The area of heat exchangers, the volume of compressor and penalty or social cost of CO_2 emission decrease with the mass flow rate, which lead to the decrease of total annual product cost.

3.2.3. *Effect of cascade temperature difference on the performance of the system*

Fig. 5 depicts the trend of the system performance with cascade temperature difference at the following conditions: T_{GEN}=363.15 K, T_{CON}=T_{ABS}=308.15 K, T_{EVA}=263.15 K, T_7=283.15 K, and ε_{SHE}=0.7. The curves in Fig. 5(a) show that the heat input of generator and the power consumption of compressor increase with ΔT_{CHE}, while COP of CACRC system decreases. This is because that condenser temperature (T_3) in the compression section and the refrigeration capacity from the absorption section increase with the increment of ΔT_{CHE}. Because the heat input of generator and the power consumption of compressor increase, COP of CACRC system decreases.

As shown in Fig. 5(b), exergy efficiency of the system decreases with ΔT_{CHE}, whereas total annual product cost decreases to minimum and then increases. The minimum total annual product cost is obtained at cascade temperature difference of 6 K. This is because the investment cost of cascade heat exchanger decreases with ΔT_{CHE}, while the investment cost of generator, absorber, condenser and compressor and penalty or social cost of CO_2 emission increase.

Table 6
Parameter settings of multi-objective optimization using NSGA-II method.

Items		Value
Population size	-	100
Pareto front population fraction	-	0.3
Maximum number of generations	-	200
Selection process	-	Tournament
Tournament size	-	2
Function tolerance	-	10^{-5}
Variable constrains	T_{GEN} (K)	337.15–373.15
-	T_{EVA} (K)	259.15–267.15
-	ΔT_{CHE} (K)	4–12
-	ε_{SHE}	0.6–0.8

3.2.4. *Effect of solution heat exchanger effectiveness on the performance of the system*

The effect of solution heat exchanger effectiveness on system performance is presented in Fig. 6 at the following conditions: T_{GEN}=363.15 K, T_{CON}=T_{ABS}=308.15 K, T_{EVA}=263.15 K, T_7=283.15 K and ΔT_{CHE}=8 K. As shown in Fig. 6(a), the heat input of generator descends and the power consumption of compressor remains stable with the increment of ε_{SHE}. The enthalpy of the weak solution entering generator increases with ε_{SHE}. However, increasing ε_{SHE} does not change the parameters of the compression section. Based on above reasons, COP and exergy efficiency of CACRC system show upward trends. It is also observed from Fig. 6(b) that the total annual product cost presents a tendency to decrease and then increase. The system achieves the minimum total annual product cost at ε_{SHE} = 0.78. The reason is that the investment cost of generator decreases with ε_{SHE}, whereas the investment cost of solution heat exchanger and absorber increase.

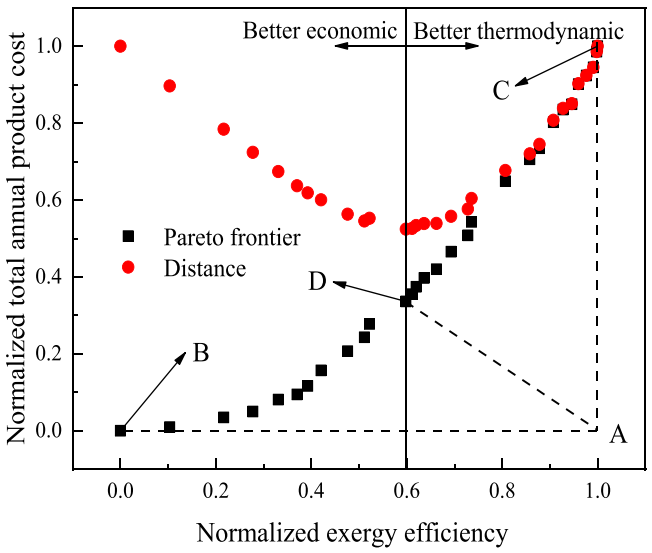

Fig. 7. Normalized form of Pareto optimal sets of multi-objective optimization for compression-absorption cascade refrigeration cycle (CACRC) system and the distance of each point in the Pareto frontier from the idea point (point A).

3.3. Optimization of the performance of the system

In order to obtain higher exergy efficiency at the expense of lower total annual product cost, non-dominated sorting genetic algorithms-II (NSGA-II) method is used for multi-objective optimization. Exergy efficiency and total annual product cost of the system are selected as target functions in this work. Parameter settings of multi-objective optimization are listed in Table 6.

Sayyaadi and Nejatolahi [21] recommended that working with the normalized data of the Pareto frontier is better than working with real values. The normalized form of target functions η_{exg} and C_T are listed below:

$$\eta_{exg,N} = \frac{\eta_{exg} - \eta_{exg,min}}{\eta_{exg,max} - \eta_{exg,min}} \tag{27}$$

$$C_N = \frac{C_T - C_{T,min}}{C_{T,max} - C_{T,min}} \tag{28}$$

where $\eta_{exg,max}$ and $\eta_{exg,min}$ are the maximum and minimum values of η_{exg} in the Pareto frontier. Besides, $C_{T,max}$ and $C_{T,min}$ represent the maximum and minimum values of C_T in the Pareto frontier.

Normalized form of Pareto optimized sets of multi-objective optimization for CACRC system and the distance of each point in the Pareto frontier from the idea point (point A) are shown in Fig. 7. The values at the point B, C and D represent the optimized results of the single-objective economic optimization, the single-objective thermodynamic optimization, and the multi-objective optimization, respectively.

Table 7 summarizes the calculated results of above three optimization scenarios. Compared to the design condition, the exergy efficiency of the system improves by 4.85%, 23.08% and 35.29% for the economic optimization, the multi-objective optimization, and the thermodynamic optimization, respectively. However, the total annual product cost decreases by 2.02% and 9.51% for multi-objective optimization and thermodynamic optimization, whereas the economic optimization increases by 7.86%. The comparison for the exergy destruction as well as the investment cost of each component in CACRC system at different optimization scenarios is given in Figs. 8 and 9, respectively. As indicated in Fig. 8, the exergy destruction of generator, absorber, and cascade heat exchanger decreases obviously after optimization, resulting the enhancement of the exergy efficiency of the CACRC system. However, the investment cost of the absorber, solution heat exchanger,

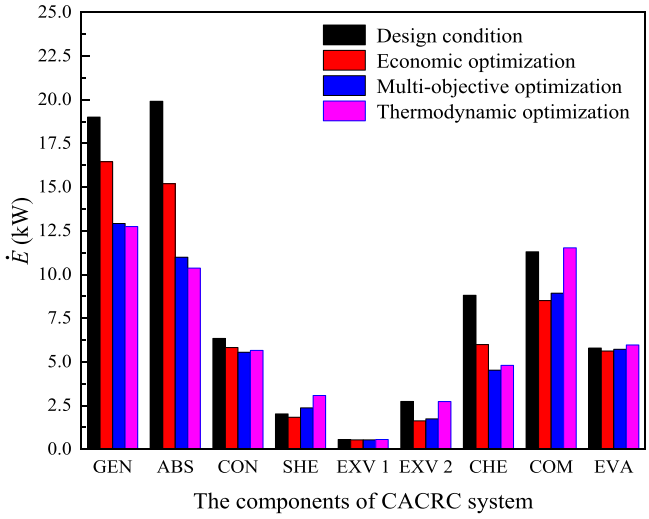

Fig. 8. Comparison of the exergy destruction of each component in compression-absorption cascade refrigeration cycle (CACRC) system.

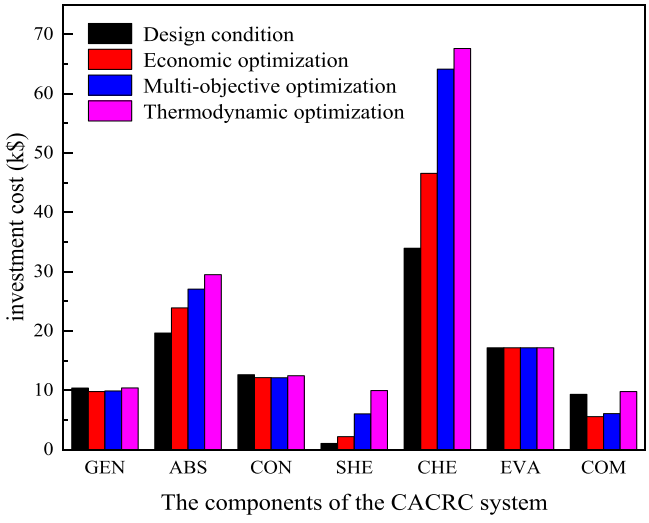

Fig. 9. Comparison of the investment cost of each component in compression-absorption cascade refrigeration cycle (CACRC) system.

Table 7
Optimized results for system.

Items	Design condition	Economic optimization	Multi-objective optimization	Thermodynamic optimization
T_{GEN} (K)	363.15	353.80	343.57	341.14
T_{EVA} (K)	263.15	267.15	264.82	259.15
ΔT_{CHE} (K)	8	5.63	4.10	4.01
ε_{SHE}	0.7	0.79	0.80	0.80
η_{exg}	0.237	0.248	0.292	0.321
C_T (k$·year^{-1})	123.27	113.58	120.78	134.99

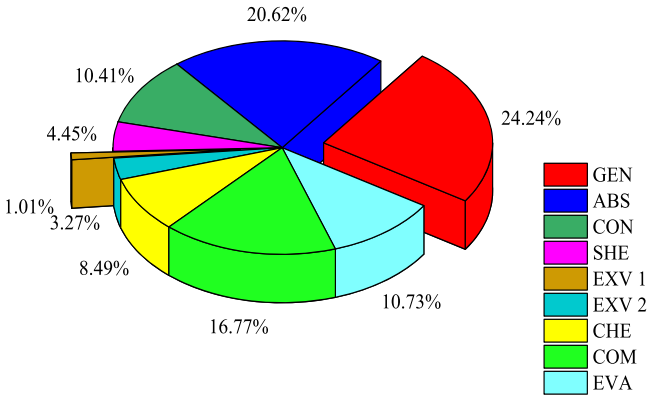

Fig. 10. Exergy destruction proportion of each component for the multi-objective optimization.

and the cascade heat exchanger increases after optimization, and other components have no obvious change.

Fig. 10 shows the exergy destruction proportion of each component for CACRC system in the multi-objective optimization. Generator has the largest exergy destruction proportion which is followed by absorber, accounting for 24.24% and 20.62%, respectively.

4. Conclusions

In this work, the performance of the CACRC system was evaluated using 16 refrigerants in vapor compression section and H_2O-LiBr in the absorption refrigeration section. Results show that the higher critical temperature and latent heat of vaporization of refrigerants in the vapor compression section, the better the performance of CACRC system. RE170/H_2O-LiBr exhibits the best performance for the CACRC system amongst all the fluids selected under the design condition. Further analysis using RE170/H_2O-LiBr indicates that the exergy efficiency of CACRC system increases firstly and then decreases with T_{GEN}, while total annual product cost decreases rapidly to minimum and then remains constant. With the increment of ΔT_{CHE} or ε_{SHE}, the system could achieve the minimum total annual product cost at 6 K and 0.78. In addition, the exergy efficiency of the system improved by 4.85%, 23.08% and 35.29% based on economic optimization, multi-objective optimization, and thermodynamic optimization, respectively.

CRediT authorship contribution statement

Yuhan Du: Investigation, Methodology, Validation, Writing – original draft. **Chenhan Chi:** Investigation, Formal analysis, Resources. **Xiaopo Wang:** Conceptualization, Supervision, Writing – review & editing.

Declaration of competing interest

The authors declare that there are no conflicts of interest.

Acknowledgments

This work was supported by the National Natural Science Foundation of China (Grant No. 51936009).

Supplementary materials

Supplementary material associated with this article can be found, in the online version, at doi:10.1016/j.enss.2024.02.003.

References

[1] J.C.V. Chinnappa, M.R. Crees, S.S. Murthy, et al., Solar-assisted vapor compression absorption cascaded air conditioning systems, Solar Energy 50 (1993) 453–458.
[2] C. Cimsit, I.T. Ozturk, Analysis of compression-absorption cascade refrigeration cycles, Appl. Therm. Eng. 40 (2012) 311–317.
[3] C. Cimsit, I.T. Ozturk, O. Kincay, Thermoeconomic optimization of LiBr/H_2O-R134a compression-absorption cascade refrigeration cycle, Appl. Therm. Eng. 76 (2015) 105–115.
[4] M.G. Gado, S. Ookawara, S. Nada, et al., Hybrid sorption-vapor compression cooling systems: a comprehensive overview, Renew. Sustain. Energy Rev. 143 (2021) 110912.
[5] Y. Khan, R.S. Mishra, Performance analysis of a solar based novel trigeneration system using cascaded vapor absorption-compression refrigeration system, Int. J. Refrig. 155 (2023) 207–218.
[6] H. Zhang, X. Pan, J. Chen, et al., Energy, exergy, economic and environmental analyses of a cascade absorption-compression refrigeration system using two stage compression with complete intercooling, Appl. Therm. Eng. 225 (2023) 120185.
[7] S. Agarwal, A. Arora, B.B. Arora, Energy and exergy analysis of vapor compression-triple effect absorption cascade refrigeration system, Eng. Sci. Technol. Int. J. 23 (2020) 635–641.
[8] M.W. Faruque, Y. Khan, M.H. Nabil, et al., Parametric analysis and optimization of a novel cascade compression-absorption refrigeration system integrated with a flash tank and a reheater, Results Eng. 17 (2023) 101008.
[9] W. Wu, B. Wang, W. Shi, et al., An overview of ammonia-based absorption chillers and heat pumps, Renew. Sustain. Energy Rev. 31 (2014) 681–707.
[10] Z. Seyfouri, M. Ameri, Analysis of integrated compression-absorption refrigeration systems powered by a microturbine, Int. J. Refrig. 35 (2012) 1639–1646.
[11] C. Cimsit, I.T. Ozturk, M. Hosoz, Second law based thermodynamic analysis of compression-absorption cascade refrigeration cycles, J. Therm. Sci. Technol. 34 (2014) 9–18.
[12] D. Colorado, V.M. Velazquez, Exergy analysis of a compression-absorption cascade system for refrigeration, Int. J. Energy Res. 37 (2013) 1851–1865.
[13] K. Salhi, M. Korichi, K.M. Ramadan, Thermodynamic and thermo-economic analysis of compression-absorption cascade refrigeration system using low-GWP HFO refrigerant powered by geothermal energy, Int. J. Refrig. 94 (2018) 214–229.
[14] M.S. Turgut, O.E. Turgut, Comparative investigation and multi objective design optimization of a cascaded vapor compression absorption refrigeration system operating with different refrigerants in the vapor compression cycle, Heat Mass Transf. 55 (2019) 467–488.
[15] A. Sencan, K.A. Yakut, S.A. Kalogirou, Exergy analysis of lithium bromide/water absorption systems, Renew. Energy 30 (2005) 645–657.
[16] R. Gomri, R. Hakimi, Second law analysis of double effect vapour absorption cooler system, Energy Convers. Manage. 49 (2008) 3343–3348.
[17] E.W. Lemmon, M.L. Huber, M.O. McLinden, NIST Standard Reference Database 23: Reference fluid Thermodynamic and Transport properties—REFPROP, Version 10.0, National Institute of Standards and Technology, Boulder, USA, 2018.
[18] J. Patek, J. Klomfar, A computationally effective formulation of the thermodynamic properties of LiBr-H_2O solutions from 273 to 500 K over full composition range, Int. J. Refrig. 29 (2006) 566–578.
[19] V. Jain, G. Sachdeva, S.S. Kachhwaha, et al., Thermo-economic and environmental analyses based multi-objective optimization of vapor compression-absorption cascaded refrigeration system using NSGA-II technique, Energy Convers. Manage. 113 (2016) 230–242.
[20] V. Jain, G. Sachdeva, S.S. Kachhwaha, NLP model based thermoeconomic optimization of vapor compression-absorption cascaded refrigeration system, Energy Convers. Manage. 93 (2015) 49–62.
[21] H. Sayyaadi, M. Nejatolahi, Multi-objective optimization of a cooling tower assisted vapor compression refrigeration system, Int. J. Refrig. 34 (2011) 243–256.
[22] M. Aminyavari, B. Najafi, A. Shirazi, et al., Exergetic, economic and environmental (3E) analyses, and multiobjective optimization of a CO_2/NH_3 cascade refrigeration system, Appl. Therm. Eng. 65 (2014) 42–50.
[23] C. Rubio-Maya, J.J. Pacheco-Ibarra, J.M. Belman-Flores, et al., NLP model of a LiBr-H_2O absorption refrigeration system for the minimization of the annual operating cost, Appl. Therm. Eng. 37 (2012) 10–18.
[24] X.L. Luo, Y.Z. Wang, J. Zhao, et al., Grey relational analysis of an integrated cascade utilization system of geothermal water, Int. J. Green Energy 13 (2016) 14–27.
[25] S.F. Mussati, T. Morosuk, M.C. Mussati, Superstructure-based optimization of vapor compression-absorption cascade refrigeration systems, Entropy 22 (2020) 428.
[26] V. Jain, N. Sharma, G. Sachdeva, et al., Performance analysis and multi-objective optimization of cooling tower assisted vapor compression-absorption cascaded and hybrid refrigeration systems, Int. J. Green Energy 16 (2019) 1024–1045.
[27] J. Wang, Z. Zhai, Y. Jing, et al., Particle swarm optimization for redundant building cooling heating and power system, Appl. Energy 87 (2010) 3668–3679.
[28] J.M. Calm, G.C. Hourahan, Physical, safety, and environmental data for current and alternative refrigerants, in: in: 23rd IIR International Congress of Refrigeration, Prague, Czech, 2011.
[29] H. Tian, G. Shu, H. Wei, et al., Fluids and parameters optimization for the organic Rankine cycles (ORCs) used in exhaust heat recovery of Internal Combustion Engine (ICE), Energy 47 (2012) 125–136.
[30] A. Ustaoglu, Parametric study of absorption refrigeration with vapor compression refrigeration cycle using wet, isentropic and azeotropic working fluids: conventional and advanced exergy approach, Energy 201 (2020) 117491.